The role of twinning in shape evolution of anisotropic noble metal nanostructures†‡

Jose Luis Elechiguerra,[a] Jose Reyes-Gasga[b] and Miguel Jose Yacaman*[a]

Received 19th May 2006, Accepted 11th July 2006
First published as an Advance Article on the web 8th August 2006
DOI: 10.1039/b607128g

Nanotechnology provides the ability to engineer the properties of materials by controlling their size and shape. Among the most interesting nanostructures are anisotropic noble metal nanocrystals such as nanorods and nanowires. Nevertheless, the production of such crystals in a controlled fashion remains as a challenging task, and many available colloidal techniques produce a mixture of morphologies. In cases where high yields of a particular anisotropic structure have been produced, the growth mechanism has been primarily explained in terms of the presence of surfactants or capping agents that regulate the growth of the crystal in a particular direction. However, the growth mechanism should also consider nucleation and kinetics, and not only thermodynamics or physical restrictions imposed by the surface stabilizing agent. In this work, we present several examples of anisotropic noble metal nanocrystals obtained by different methods. Finally, the important role of twinning in determining the habit of the final morphology is discussed.

1. Introduction

Noble metal nanostructures have drawn increasing interest due to potential applications in catalysis, biology, and electronics among others.[1,2] As these materials have at least one dimension between 1 nm and 100 nm, their physicochemical properties are highly influenced by shape and size.[3] For example, for nearly a century, it has been known that the number, location, and intensity of surface plasmon resonance (SPR) bands of gold and silver nanoparticles are strongly correlated with both the shape and size of the particle.[4] Recently, the absorption spectra of individual silver

[a]*Department of Chemical Engineering and Texas Materials Institute, The University of Texas at Austin, Austin, Texas 78712, USA. E-mail: josee@che.utexas.edu; yacaman@che.utexas.edu; Fax: +1-512-471–7060; Tel: +1-512-232-9111*
[b]*Instituto de Física, Universidad Nacional Autónoma de México, Apartado Postal 20-364, 01000 México, D.F., México. E-mail: jreyes@fisica.unam.mx*
† This paper is part of a *Journal of Materials Chemistry* theme issue on Anisotropic Nanomaterials. Guest editor: Luis Liz-Marzan.
‡ Electronic supplementary information (ESI) available: experimental procedure. See DOI: 10.1039/b607128g

Jose Luis Elechiguerra

Jose Luis Elechiguerra Joven attended the National Autonomous University of Mexico and obtained a Bachelor of Chemical Engineering degree in May of 2001. In August of 2002, he entered graduate school at the University of Texas at Austin in the Department of Chemical Engineering and pursued his PhD under the advisement of Dr Miguel Jose Yacaman, where he obtained a MSE degree in December of 2004 and a PhD degree in April 2006. Currently, he is working for McKinsey & Co. in Mexico City.

He received his BS and PhD in Physics from the National University of Mexico in 1968 and 1973 respectively. Most of his PhD work was done under Nicolas Cabrera in Mexico and under Alan Bassett in Warwick, UK. He did his post doc at Oxford University under Peter Hirsh and in Nasa Ames under Helmut Popa. He was a professor of The Institute of Physics at The National University of Mexico until 2002. He joined The University of Texas at Austin in 2002 as Reese Endowed Professor in Engineering at the Chemical Engineering Department. He leads a research group in Nanotechnology and has been a world leader in the field of nanoparticles including growth and characterization by electron microscopy techniques; with more than 350 scientific papers in this field. Professor Yacaman has served as Director of Science of the National Council of Science and Technology of Mexico and Director of The Nuclear Research Institute of Mexico. He is a Member of The National Academy of Sciences of Mexico, and has received numerous awards.

Miguel Jose Yacaman

nanoparticles were correlated with their size and shape determined by transmission electron microscopy (TEM).[5] The results indicated that spherical and roughly spherical nanoparticles absorb in the blue region of the spectrum, while decahedral nanoparticles and particles with triangular cross sections absorb in the green and red part of the spectrum, respectively. For each different morphology, the SPR absorption wavelength increased with size. In addition, it is also known that, as the aspect ratio of the nanocrystal increases such as in the case of nanorods and nanowires, the SPR splits into two bands: the high energy band corresponding to the oscillation of the electrons perpendicular to the major axis of the nanocrystal (transverse plasmon absorption), and the lower energy band relating to the oscillation of the electrons along the major axis of the nanocrystal (longitudinal plasmon absorption). Moreover, anisotropic noble metal nanocrystals are excellent substrates for surface enhanced Raman spectroscopy (SERS); by adjusting the shape and aspect ratio of the crystal, the surface plasmon resonance can be tuned to resonate with a laser and optimize the electromagnetic enhancement.[6] In catalysis, it has been established that both reactivity and selectivity of platinum nanoparticles in a catalytic reaction are strongly dependent on the crystallographic planes exposed on the surfaces of the nanocrystals.[7] Thereby, to tailor the properties of noble-metal nanomaterials, exquisite control of size and morphology is highly desirable.

As a consequence, the development of synthesis methods that allow control of both the size and the shape of the nanocrystals is a major subject for research. Nowadays, metal nanoparticles can be fabricated with many different techniques. Among the most commonly used techniques for producing arbitrary patterns of nanoparticles for many technological and scientific applications are lithographic techniques such as electron beam lithography (EBL), nanosphere lithography (NSL) and focus-ion beam lithography (FIB), among others.[8] Nevertheless, despite all the advantages that some of these techniques have, the synthesis of inorganic nanomaterials *via* soft-chemical colloidal techniques has been demonstrated to be the most effective, reliable and versatile route for their production. While significant achievements for the size-controlled synthesis of noble-metal nanoparticles have been made,[1] only limited progress that deals with effective shape-controlled colloidal synthesis of these nanocrystals in high yields has been made, particularly regarding the production of anisotropic nanostructures.

Because of the high symmetry of the fcc system, forcing noble-metal colloidal particles to acquire a non-spherical shape is not an easy matter, and involves a competition against the desire of the systems to minimize the surface area energy through the formation of spherical particles.[9] Therefore, the most common morphologies are isotropic particles, ranging from quasi-spherical to highly faceted particles, typically being octahedral or cubic in shape. Nevertheless, several reports on the synthesis of gold,[10–12] silver[13–16] and copper[17,18] nanorods and nanowires have recently appeared, and two dimensional colloids such as triangular and hexagonal prisms of different thickness and aspect ratios have also been reported in numerous papers.[19]

It is interesting that nearly identical shapes and habits tend to appear from radically different synthesis methods. However, almost independently of the differences in reaction methods, the production of these thermodynamically unfavorable morphologies has been explained by the particular reaction environment, highlighting primarily the fundamental role of capping agent molecules in directing the anisotropic structures, rationalized mostly by two ideas.[6] The first explanation proposes that preferential absorption of capping agent molecules inhibits the addition of metal atoms to specific crystal faces. The second idea suggests that high concentrations of surfactant promote the formation of micelles that act as quasi-hard templates for the metal crystal growth. Nevertheless, both explanations are unable to address many experimental observations. In fact, some of these shapes have been observed in crystals grown by evaporation in vacuum, where no capping agent or solution was used.[20] Foremost, in most of the available synthesis methods, there is a high diversity of shapes in a single homogeneous reaction environment, and the reaction products generally consist of a mixture of isotropic particles with a small portion of anisotropic ones. Even in selected examples where high yields of a particular anisotropic morphology have been achieved, such as the case of the silver nanowires produced by the polyol method in the presence of poly(vinyl pyrrolidone) (PVP),[14] great care needs to be taken to reproduce the results from batch to batch. It is highly probable that the capping agent, under specific reaction conditions, is truly helping to increase the yield of a particular structure, but the growth mechanism should also consider nucleation and kinetics, and not only thermodynamics or physical constrictions imposed by the surface modifying agent. Bearing this in mind, Lofton and Sigmund proposed a growth mechanism derived from the growth of silver halide crystals.[21] Their suggestion relies on the formation of twin planes that promote the creation of favorable sites for further growth, leading to anisotropic growth. Indeed, the formation of twins during nucleation and growth of colloidal noble-metal crystals is expected for most reaction environments and conditions. According to reasons that will become apparent as this discussion continues, the particular structure of several of the most characteristic anisotropic morphologies for noble metal nanostructures will be discussed on the basis of this model. Additionally, examples of how the particular structure of the material modifies its properties are also provided.

2. Small nanoparticles

2.1 Structural fluctuations in small nanoparticles

During the last couple of years it has been established that, in the case of colloidal synthesis of nanocrystals, the structure of the original seeds plays a crucial role in the morphology of the final product. Numerous TEM studies on small ($\leqslant$5 nm) metal particles have demonstrated that slight excitations, even at room temperature, are sufficient to induce structural fluctuations within the nanoparticle, and that the rates of such oscillations increase with the decreasing size of the nanocrystals (Fig. 1).[22,23] Based on these observations and the results of theoretical calculations, it is known that the total potential surface energy for the different nanoparticle morphologies

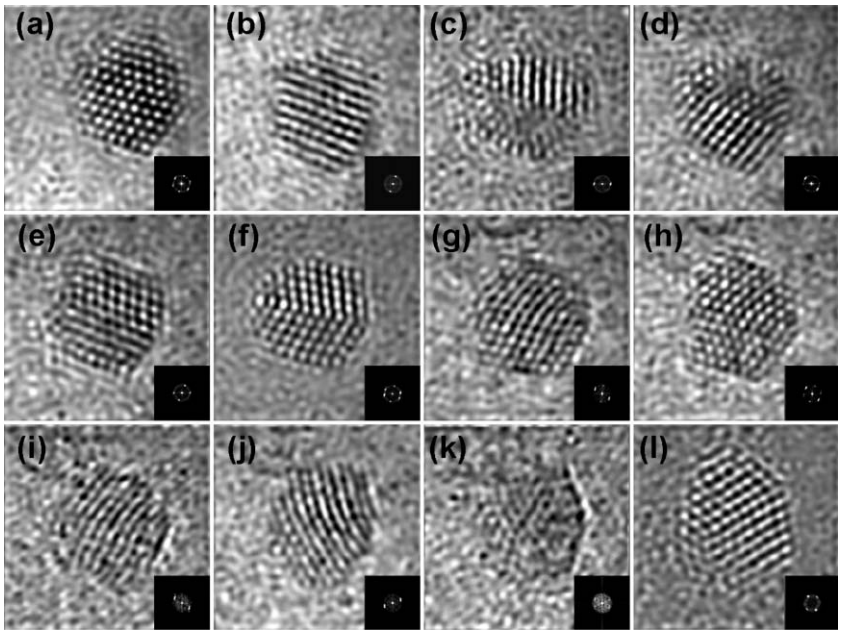

Fig. 1 Fluxional character of small noble metal nanoparticles. TEM images and their corresponding FFTs of the same gold nanoparticle at different times.

consists of several minima, and that the energy barriers between them are low enough ($\sim kT$); hence, thermal fluctuations provide sufficient energy to produce changes between the different morphologies. At these small sizes, the five-fold symmetry twinned structures such as icosahedra and decahedra tend to be slightly more stable, while cuboctahedral nanoparticles become more stable at larger sizes.[22] Therefore, it is almost impossible to effectively control the shape of small nanoparticles. However, as the size of the crystal increases, the rate of structural fluctuations decreases, thus fixing the nanoparticle morphology either as single-crystalline or multi-twinned, and control over shape is then achievable. On the basis of this model, one can easily understand why in a typical sample of nanoparticles produced by most of the solution phase techniques, a statistical distribution of shapes will be observed. However, some progress has been achieved in controlling the shape and size of larger metal nanostructures, and many applications have been proposed based on their morphology.[6,24,25]

2.2 Structure of small nanoparticles

In the case of highly symmetric fcc metals, the surface energy of the different faces is rather uniform and typically isotropic particles are generated. Indeed, the shape of a single-crystal fcc material should by defined by its Wulff shape, where the equilibrium shape of a particle in free space is determined by minimizing the surface energy. For a crystalline material, such as the case of noble metals, the Wulff condition predicts a single crystalline polyhedron.[26] For fcc crystals the relative surface energies of the low-index crystallographic planes are $\gamma_{111} < \gamma_{100} < \gamma_{110}$. Additionally, if $\gamma_{110}/\gamma_{111} \geqslant \sqrt{(3/2)}$, the Wulff polyhedron correspond to a truncated octahedron with eight (111) and six (100) faces (Fig. 2a). In the case where $\gamma_{110}/\gamma_{111} \geqslant \sqrt{(3/2)}$ is not satisfied, (110) truncations at the edges where two (111) faces came together should be introduced (Fig. 2b). However, it has been demonstrated that, in the case of small nanoparticles, this equilibrium shape is not exclusively observed and multi-twinned nanoparticles (MTPs), especially with five-fold symmetry, are also present (Fig. 2c–e).

Pentagonal arrangement in MTPs is quite well known and five-fold symmetry nanoparticles have provoked much attention during the last 50 years. Indeed, multi-twinned nanoparticles of transition metals with fcc lattice[27] and some related materials such as carbon[28] and germanium have been reported.[29] Five-fold twinning is not only found in synthetic materials, but also in structures with a natural origin (for an excellent review, please consult reference 30). The pioneering work of Ino and Ogawa described gold nanoparticles with icosahedral and decahedral structures in terms of a multi-twinned model.[30] Based on those studies, the basic structure of a decahedral particle can be described as the junction of five

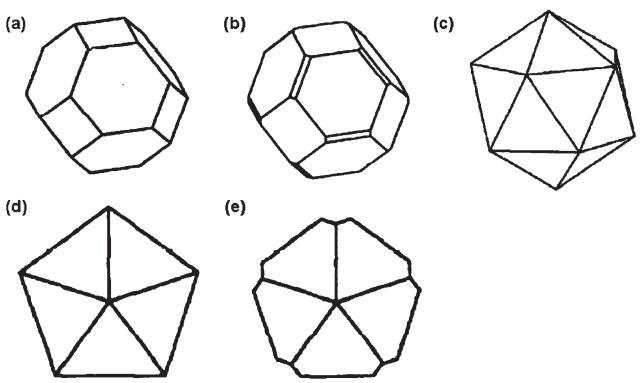

Fig. 2 Most common morphologies for small metal nanoparticles: (a) truncated octahedron, (b) truncated octahedron with extra (110) truncations, (c) icosahedron, (d) regular decahedron, and (e) Mark's decahedron.

tetrahedral single crystals with twin-related adjoining faces. Later on, motivated by experimental observations, Marks proposed the existence of reentrant only {111} facets at the twin boundaries of the decahedron, thus decreasing its surface energy (Fig. 2e).[31]

Importantly, the theoretical angle between two (111) planes is 70.52°, so by joining 5 tetrahedrons, which are bounded by {111} facets, a gap of 7.40° is generated. Thus, the space can not be filled just by joining five tetrahedra and some form of internal strain is necessary, giving rise to dislocations and other structural defects. Similarly in an icosahedral particle, formed by the junction of 20 tetrahedra, internal strain is required to close the gaps formed because of the multi-twinned nature of the structure. Macroscopic, as well as microscopic, theoretical calculations have shown that at small sizes, the extra energy introduced in the particle due to stacking faults and strain, caused by the twins and the generated gap, is readily compensated by maximizing the amount of high-density {111} planes; yet, as the particle grows in size, the exposure of only {111} can not compensate for the excessive strain energy required to sustain the multi-twinned structure and the particle progresses into an fcc-type structure.[32] Consequently, it has been predicted that five-fold-type particles are thermodynamically favored primarily at very small sizes (less than 20 nm) and that, as the size of the particle increases, the structure should evolve into an fcc-type particle, such as a cuboctahedron. However, this is not always the case and non-thermodynamically stable shapes have also been observed at larger sizes.[33] Hence, it appears that a strictly thermodynamic explanation can not be used, but that the kinetics of growth, starting with the size, shape and structure of the nuclei, should play a critical role in determining the habit of the final product. In particular, as has been previously reported, twinning plays an important role in shape evolution.[20,21]

2.3 Twins

Twins, as well as stacking faults, are readily formed during crystal growth in materials with low stacking fault energy,[34] such as gold and silver. Twins could form as a result of atoms erroneously attached to a growing crystal in such a way that two crystals appear to be growing out of each other (Fig. 3a). In this context, two general types of twinning exist: contact and penetration. In the case of contact repeated twinning, either lamellar or cyclic, the habit of the crystal is seriously affected.[35] When parallel twins are repeated continuously one after another lamellar twinning is formed (Fig. 3b), while cyclic twinning requires nonparallel coplanar composition planes. In this case, a complete circle can be formed such as the case of the five-fold symmetry nanoparticles (Fig. 3c). This type of five-fold multiple twinning is favored for fcc crystals with low twin boundary energy and surface energy anisotropy, just as in the cases of several transition metals.

3. Colloidal synthesis of anisotropic noble metal nanostructures

As mentioned earlier, chemical syntheses offer a versatile route to assembling atoms and particles from the atomic or molecular state to the macroscopic scale, thus allowing tailoring of the properties of materials in what is known as the bottom-up approach. In addition to the atomic structure, the characteristics of the crystals basically depend on the composition, microstructure, defects, and interfaces, which can be controlled by thermodynamics and kinetics of the synthesis.[36] In the present discussion, we present several examples of anisotropic materials, synthesized by different methods.

Murphy and co-workers have intensively synthesized gold and silver nanorods and nanowires in the presence of cetyltrimethylammonium bromide (CTAB), in what is known as the seed-mediated technique.[6,12,13] Pileni has demonstrated that anisotropic copper nanostructures can be produced in the presence of reverse micelles of AOT (sodium bis(2-ethylhexyl) sulfosuccinate).[17,18] Among solution phase techniques, the polyol method is one of the most employed routes for the synthesis of metal nanostructures. This method has been successfully employed for the production of noble-metal nanostructures with controlled shapes such as nanocubes, nanowires, and spherical nanoparticles including the synthesis of bimetallic alloys and core–shell nanoparticles.[14,33,37,38] In the case of silver, Xia *et al.* demonstrated that by carefully adjusting the molar ratio between silver nitrate and PVP, a range of controlled morphologies such as nanocubes and nanowires can be produced.[24] They found that if single-crystalline seeds were primarily produced, the final product is composed of monodispersed cubes, tetrahedra and octahedra, while if multi-twinned particles with decahedral shape were primarily formed, the final product is mainly composed of nanorods and nanowires with a remarkable multi-twinned structure with pentagonal cross sections. Furthermore, we recently reported a novel and simple approach to control the

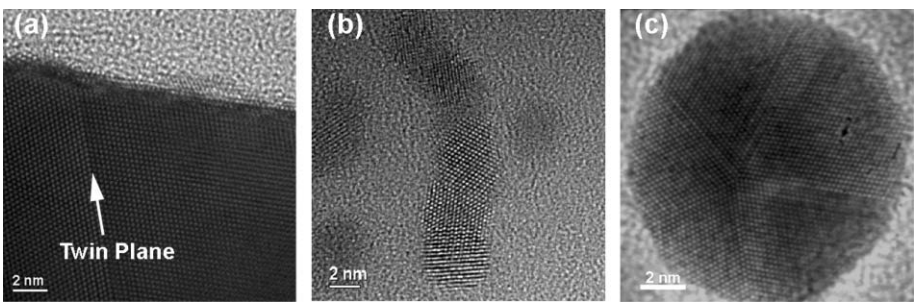

Fig. 3 Examples of contact twinning in small particles: (a) silver nanoparticle particle with a single twin, (b) gold nanoparticle with lamellar twins, and (c) decahedral gold nanoparticle (cyclic twinning).

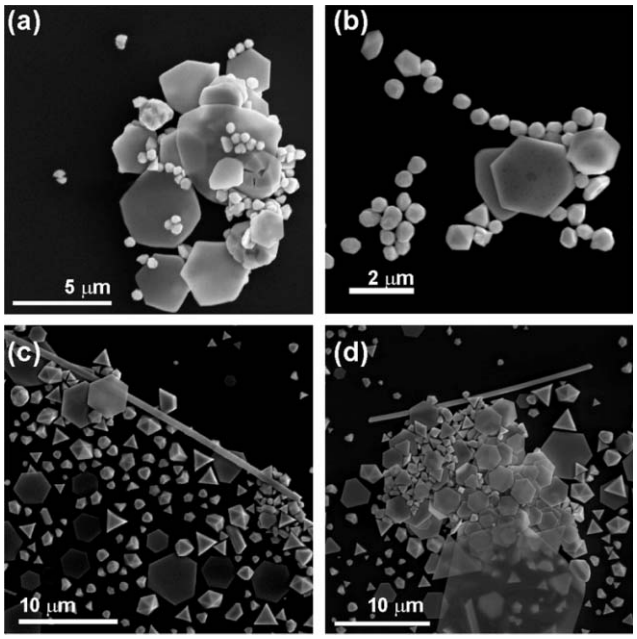

Fig. 4 SEM images of the products obtained by decreasing the addition rate of the gold precursor solution from 0.3750 mL min^{-1} to 0.1875 mL min^{-1}. (a, b) Product obtained at 160 °C. (c, d) Product obtained at 200 °C.

reduction kinetics of a Pt precursor using the polyol method in glycerin by replacing the use of PVP by poly(diallyldimethylammonium chloride) (PDDA).[39] As PDDA is a cationic polyelectrolyte, the initial strong electrostatic interaction between PDDA and the anionic metal precursor results in the formation of stable ion pairs. Therefore, by varying the ratio between capping agent and metallic precursor as well as the concentration of Pt in the initial solution, the kinetics of the reaction can be manipulated and several morphologies can be obtained including spherical polycrystalline submicron- and nano-particles as well as branched nanocrystals.

By using the same simple approach to control the kinetics of the polyol method, we obtained gold colloids with different morphologies and crystallinity. For a complete description of the obtained products, as well as the detailed experimental conditions, please refer to the electronic supplementary information (ESI‡). Briefly, when an addition rate of chloroauric acid solution of 0.375 mL min^{-1} was used, an agglomeration growth mode was encouraged and polycrystalline sub-micron gold particles were obtained. To promote a diffusional mode of growth, the addition rate of the chloroauric acid solution was decreased to 0.1875 mL min^{-1}. In this case, instead of polycrystalline particles, the product of the reaction was composed of well defined faceted crystals including triangular and hexagonal platelets and polyhedral particles, although, from SEM images, it is clear that the crystals were not perfectly formed and many defects on their surfaces are clearly observed (Fig. 4a and b). To improve the quality of the obtained crystals and promote the formation of more defined polyhedral shapes, the temperature of the reaction was increased from 160 °C to 200 °C, maintaining the same addition rate and amount of PDDA as in the previous case (Fig. 4c and d). Again, the product of the reaction was a mixture of faceted particles with well defined faces and edges. Apparently, by increasing the temperature of the reaction, the diffusion of metal atoms into the surfaces of the initially formed crystals was enhanced and crystals with a higher quality were obtained. Fig. 5 shows SEM images of the most characteristic morphologies: nanowires with pentagonal cross-sections, decahedral particles, cubic particles, octahedral particles, tetrahedral and truncated tetrahedral particles, and different triangular and hexagonal platelets.

3.1 Isotropic particles

As mentioned previously, in the case of highly symmetric fcc metals, the surface energy of the different faces is rather uniform and typically isotropic particles are generated; for instance, a cube of all {100} faces, an octahedron of all {111} or their truncations to form a cuboctahedron with {100} and {111} faces. As seen in Fig. 6, several cubes with a dimension of approximately 500 nm were produced. Electron diffraction

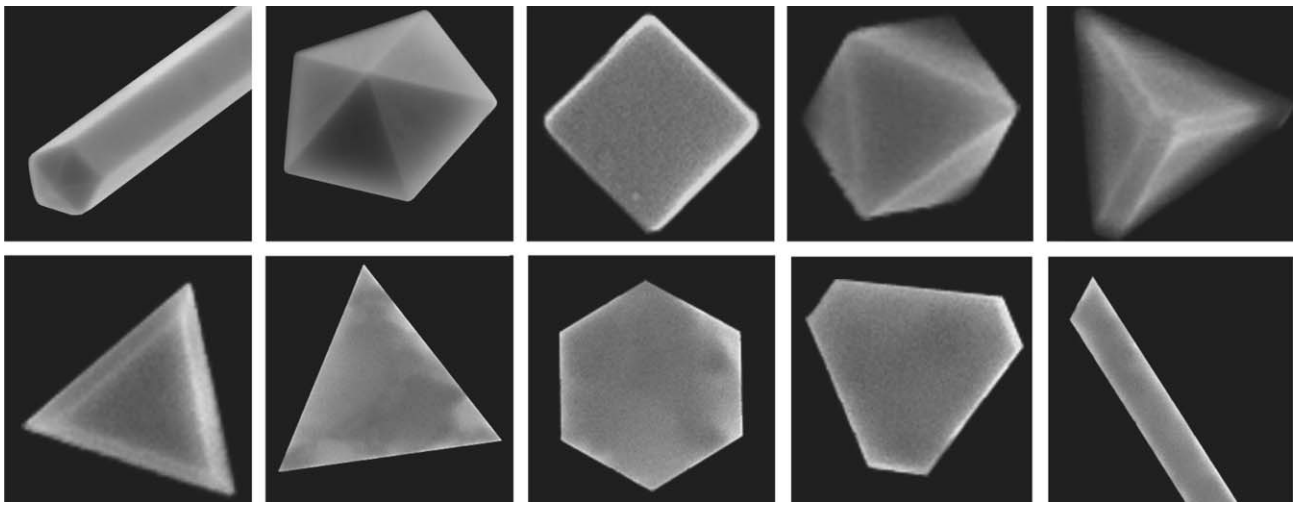

Fig. 5 SEM images of the most characteristic morphologies: pentagonal cross-section nanowires, decahedral particles, cubic particles, octahedral particles, tetrahedral and truncated tetrahedral particles, and platelets with different shapes.

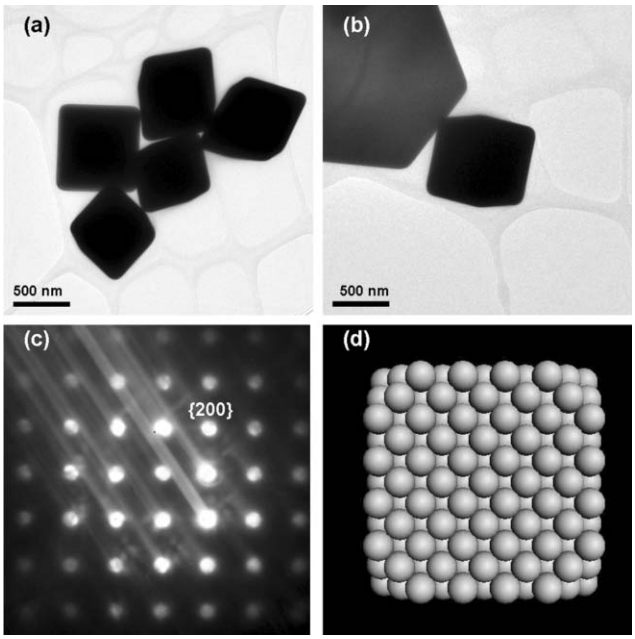

Fig. 6 Cubic particles. (a, b) TEM images of gold cubic particles. (c) Electron diffraction pattern of one cubic particle. According to this, the particles are single crystals primarily bounded by {100} facets. (d) Schematic model of this type of particle.

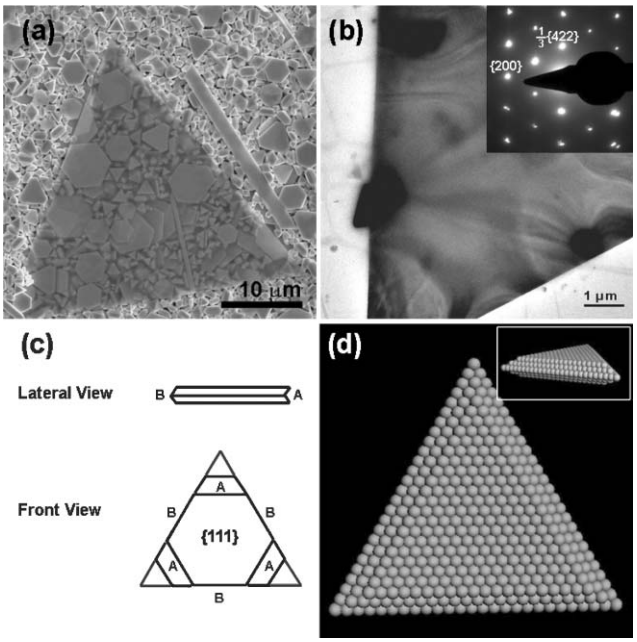

Fig. 7 (a) SEM and (b) TEM image of one gold triangular platelet. The inset shows a selected area electron diffraction pattern of the same particle. (c) Growth model for a single twin plane platelet. Adapted from reference 21. (d) Schematic model of this type of particle.

of a smaller single particle showed that the cube is a single domain, primarily bounded by {100} faces. The corners of such particles were slightly truncated exposing {111} faces. Other isotropic-type particles were also seen, such as the octahedral particle depicted in Fig. 5. In this case, the surfaces of these type of particles are dominated by {111} faces, which render them energetically favorable compared to prisms with other high-energy surfaces such as $(1\bar{1}0)$ and $(11\bar{2})$.

3.2 Anisotropic particles

3.2.1 Hexagonal and triangular platelets. Two of the most common morphologies were 2D platelets either triangular (with and without truncated corners) or hexagonal in shape. In some cases, the aspect ratio of these platelets was as high as 100 : 1 with side lengths up to ~40 μm. This type of platelet structure has been reported for many other synthesis techniques and for other metals such as silver.[19] Due to their flat surfaces, sharp corners and smooth edges, these structures tended to be oriented in the <111> direction. The selected area electron diffraction pattern of the triangular platelet of high aspect ratio, shown in Fig. 7b, confirmed the presence of the {220} reflection for the lattice planes of gold, verifying that they are primarily bounded by {111} faces. Additionally, the inner circle of spots corresponded to the ⅓{422} reflection. These spots are forbidden in a single-crystal fcc metal, but can appear when two twin planes are parallel to one another. It is worth mentioning that this type of reflection is also observable from atomically flat surfaces of gold and silver.[24]

As explained by Lofton and Sigmund,[21] anisotropic prisms with hexagonal and triangular shapes have been also synthesized for the silver halide system and have been extensively characterized because of their importance in photographic technology. The growth of such prisms in the silver halide system has been explained in terms of the formation of twin planes in the [111]-type faces (Fig. 7c). Since silver and gold have the lowest stacking fault energies among metals, the energy to form a twin plane is decreased and twins readily form. Because of the sixfold symmetry of the fcc system, these twinned crystals should form hexagonally-outlined nuclei. Indeed, the hexagonal platelets that remained in the system might be explained as nuclei for triangular platelets where growth was inhibited due to the exhausted amount of available gold in the reaction media. Once the hexagonal prisms are formed, at the six surfaces where the twin plane ends, the stacking fault of such plane causes {111} faces to form in an alternating concave and convex fashion (Fig. 7c), namely A and B types respectively. In the case of the convex type surfaces, any extra added atom has limited stability due to the presence of only three nearest atomic neighbors and, therefore, the re-dissolution of that atom into the reaction media is likely to occur. Therefore, for a new layer to be added in these surfaces, an energy barrier must be overcome and, in the absence of a dislocation or defect, the growth of these surfaces will be very slow. On the other hand, the concave surfaces creates re-entrant grooves that increase the number of nearest atomic neighbors providing extra stability and promoting faster growth. In a crystal with only a single twin, since the concave sides are bounded by slow-growing convex sides, they grow out of existence leaving a triangular prism of a size defined by the size of the original particle at the time of the twinning event. A schematic model of such a prism is depicted in Fig. 7d, where a single twin plane perpendicular to the [111] direction is shown.

Platelets with lower aspect ratios (width : thickness), can be explained by the creation of a single twin rotated by 60° relative to the first twin plane; thus, preventing the convex

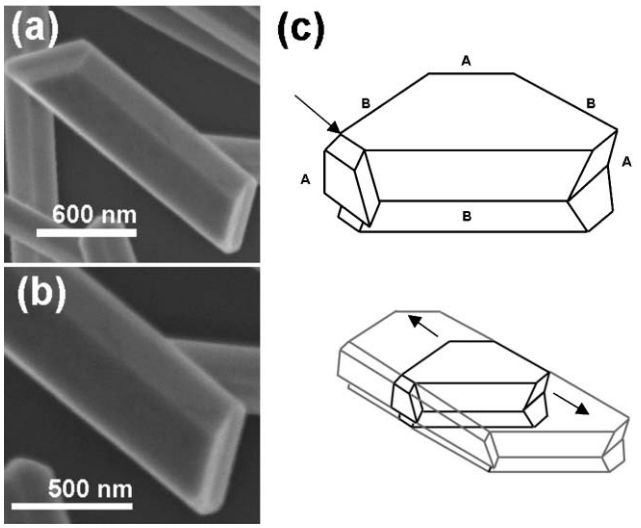

Fig. 8 Rod-like platelet. (a, b) SEM images of a wire-like platelet. (c) Growth mechanism based on the creation of a second twinning event on a fast-growing concave face. Adapted from reference 21.

faces from growing out, leading to sustained growth in two dimensions. However, if the second twin plane forms at an obtuse angle relative to the first twin plane on one of the fast-growing concave faces, the particle will grow rapidly in one direction and form a rod-like particle. An example of this case is shown in Fig. 8.

As illustrated in Fig. 8c, after the formation of the first twin plane, a second twin plane (marked by the arrow) formed on one of the re-entrant (111) planes blocks further growth and generates two new fast concave growing faces. As material is added to both grooves, uniaxial growth is achieved.

3.2.2 Decahedral particles and nanowires with pentagonal cross-sections. As exemplified in Fig. 9, decahedral particles of very large ($\sim$1 μm) sizes were also observed. As discussed earlier, theoretical calculations have shown that this structure is favorable primarily at nanometric sizes. Hence, it is quite surprising that micrometric decahedra were obtained. A possible explanation might be the presence of inhomogeneous strain at the interface. In most of the theoretical calculations, the strain required to fill the space is homogeneously distributed through the decahedral structure; yet, if dislocations are present, the strain energy is decreased and the particle can grow larger than those predicted sizes. We have observed the presence of partial dislocations, which result from the intersection of two stacking faults in different planes that met along the boundary. In the case of small decahedral

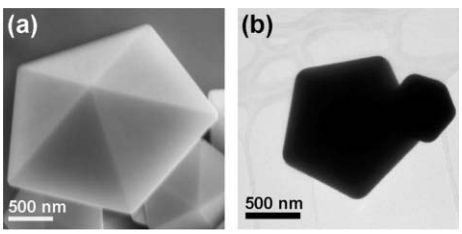

Fig. 9 (a) SEM and (b) TEM images of large decahedral particles.

nanoparticles, as shown by de Wit,[40] a positive wedge disclination produced at the center of the nanoparticle because of the circular stacking of twinned tetrahedral units can close the gap of 7.40°. However, many times just four of the twin boundaries are coherent, suggesting that most of the strain is localized in just one boundary between two grains.

Because of the size of these particles, it was not possible to obtain quality electron diffraction patterns. However, the fast Fourier transform (FFT) of a small decahedral gold nanoparticle shown in Fig. 10b exemplifies the type of electron diffraction pattern obtained for this kind of nanocrystal. For clarity, a model for a decahedral nanoparticle was created, and its corresponding electron diffraction pattern in the [110] direction, perpendicular to the five-fold symmetry axis, was simulated. This complex and remarkable diffraction pattern can be well interpreted by the superposition of five subcrystals related to face-centered cubic gold crystals with a [110] orientation, and each diffraction spot can be simply attributed to a specific subcrystal. In other words, as the decahedron is formed by five tetrahedra with twin-related adjoining faces, by superimposing the [110] direction electron diffraction pattern

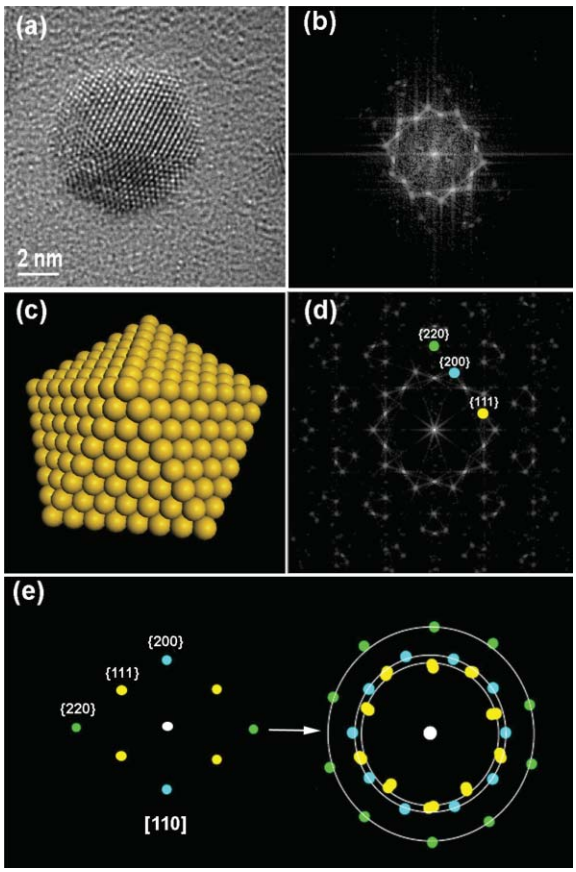

Fig. 10 (a) HRTEM image of a decahedral gold nanoparticle. (b) Fast Fourier transform (FFT) of the nanoparticle shown in (a). (c) Schematic model of a decahedral gold particle. (d) Simulated electron diffraction pattern of the model particle shown in (c). (e) Left: Schematic [110] direction diffraction pattern for fcc gold. Right: Five [110] superimposed diffraction patterns rotated with respect to each other; the five-fold symmetry electron diffraction pattern of (d) is generated.

of each crystal rotated with respect to each other; the five-fold symmetry electron diffraction pattern of Fig. 10d is generated.

Another type of particle commonly observed was wires with pentagonal cross-sections. In this case, the final habit of the nanowires corresponds to the Johnson solid number J_{16}, *i.e.* an elongated pentagonal dipyramid.[41] This habit is analogous to the structures earlier reported by Melmed and Hayward.[42] They observed whiskers of nickel, iron and platinum with a structure composed of five twins arranged about their common [110] axis. Similarly to the decahedral particles, the wires were sufficiently thick to complicate the acquisition of good diffraction patterns. However, the silver nanowires produced by the polyol method in the presence of PVP do have the same structure and, for them, good quality selected area diffraction patterns were taken (Fig. 11). The orientation of the nanowire with respect to the electron beam is shown in the inset figures. Because of the five-fold symmetry of the structure, a rotational periodicity of 36° for each pattern was revealed. Initially, both diffraction patterns are easily interpreted as the overlapping of the [100] and [112] zone axes (Fig. 11d), and the [111] and [110] zone axes (Fig. 11e) of the silver fcc unit cell. Nevertheless, the presence of a non-periodic sequence of diffraction spots marked by arrows in Fig. 11d is relevant for the analysis, and cannot be interpreted on basis of the above simple indexation.

As stated before, in recent years, there have been recent reports about the synthesis of 1-D nanostructures of gold, silver and copper, among others. Several of these reports indicate that some of these 1-D nanostructures possess this remarkable five-fold multi-twinned structure.[16,17,43,44] As shown in Fig. 11b, their cap resembles a decahedron with a contrast quite similar to the one presented by multiple twinned decahedral particles. Based on this observation, it has been proposed that they evolved from a multi-twinned decahedral nanoparticle growing in the [110] direction with the capping agent directing the structure by stabilizing more effectively the new formed {100} facets than the {111} facets; thus, they may be considered as decahedra that have elongated parallel to the twin planes. In the case of PVP, its anisotropic binding specificity has been attributed to the difference in surface atom density between the {100} and {111} silver planes, 1.20×10^{19} *vs.* 1.38×10^{19} atoms m^{-2}, respectively.[24] However, the preferential interaction between the capping agent and different metal surfaces can not fully explain the physical mechanism that allows the formation of such a structure and allows it to be energetically stable. As mentioned earlier, a decahedron can be considered as the junction of five tetrahedra and, in that case, each vertex is the point where a fast-growing concave type face grew out, leaving five edges and two axis points as slow-growing convex faces. Thus, on the basis of that explanation, typically a fivefold particle must grow into a regular decahedron and then be arrested in growth. Yet, as speculated by Lofton and Sigmund, if an additional twinning event occurs on an undeveloped decahedron, a similar event to the platelet shown in Fig. 8 should take place. This new variant would regenerate the re-entrant grooves in the central axis and new faces would appear; thus, the sides of the wire will be formed (Fig. 12). Still, further electron microscopy and diffraction studies are needed to confirm whether this is the case.

Recently, we performed a comprehensive analysis on the structure of the silver nanowires produced by the polyol method.[45] We demonstrated that their high resolution transmission electron images (HRTEM) can be interpreted as a Moire pattern contrast based on a multi-twinned decahedron, and that their selected area electron diffraction (SAED) patterns can be also completely generated through a multi-twinned decahedral basis. In that sense, we proposed that this type of structure can be better interpreted as a chain of decahedra joined along the vertex, parallel to the five-fold

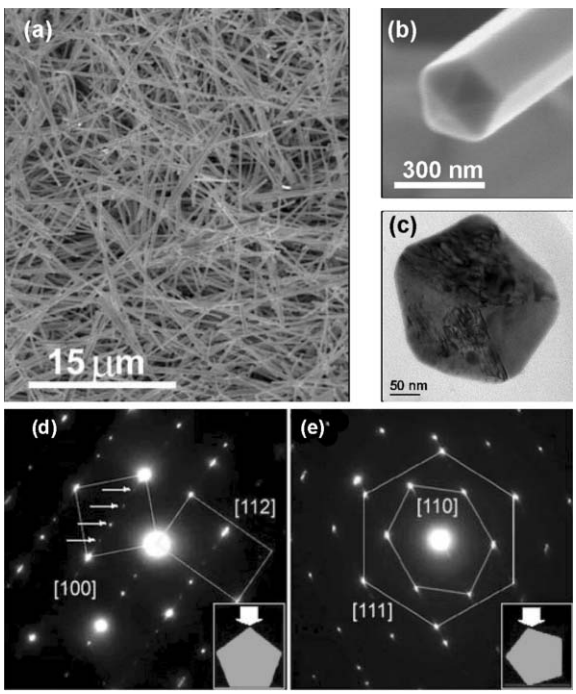

Fig. 11 (a) SEM image of the synthesized silver nanowires. (b) SEM image where the pentagonal cross-section of the nanowires can be observed. (c) TEM image of a cross-section of one silver nanowire. (d, e) Characteristic selected area electron diffraction patterns of the silver nanowires. Their indexation indicates that they correspond to the overlapping of the (d) [100] and [112] zone axes, and the overlapping of the (e) [111] and [110] zone axes, respectively. Note the existence of an aperiodic sequence of diffraction spots in (d).

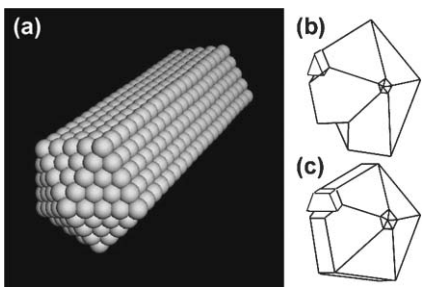

Fig. 12 (a) Schematic model of a gold wire with a pentagonal cross section. (b) Five-fold twinned particle prior to growth into a regular decahedron. If a second twining event occurs in the fast-growing concave faces, (c) the decahedron will elongate parallel to the twin planes. Adapted from reference 21.

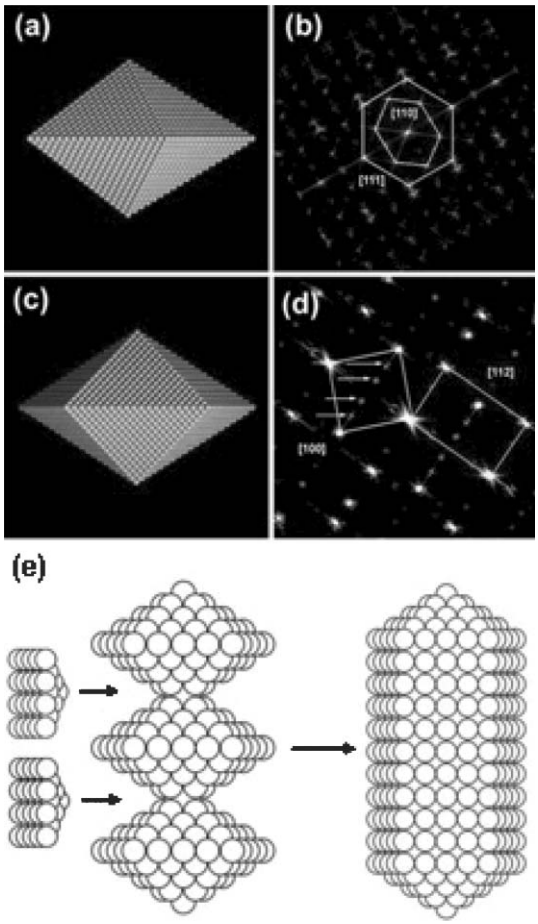

Fig. 13 (a, c) Schematic silver decahedron. This structure consists of 5 tetrahedra based on the silver fcc unit cell joined along the common [110] edge. (b) Simulated diffraction pattern along the [110] direction. (d) Simulated diffraction pattern along [100]. (e) Schematic representation of the polyhedra formed by our model based on a chain of decahedra. The decahedra are brought together to form a chain along the vertex, or the tetrahedra common edge [110].

symmetry axis. As shown in Fig. 13, a model for a multi-twinned silver decahedron was generated and the corresponding electron diffraction patterns along the same directions as the experimental ones were simulated. It should be clarified that the model in Fig. 13 is not a growth model but it is intended for calculating diffraction patterns. It is clear that all the features, including the aperiodic sequence of spots, are observed. Actually, the diffracted spots in the simulated patterns are similar in position and intensity to the experimental patterns. Therefore, it is reasonable to conclude that the observed aperiodic sequence is produced by the twinning relationship of the five crystals that compose the decahedral-like cross section of the nanostructure. Indeed, the aperiodic sequence is formed by the combination of double diffraction (directly related with the multi-twinned structure of the nanowire) and by the small size (*i.e.* nano) of the wire, since spots from the first order Laue zone (FOLZ) are also present (Fig. 14).

Interestingly, when the temperature of the reaction media was increased from 160 °C to 200 °C, large aggregates precipitated from the reaction flask. Scanning electron

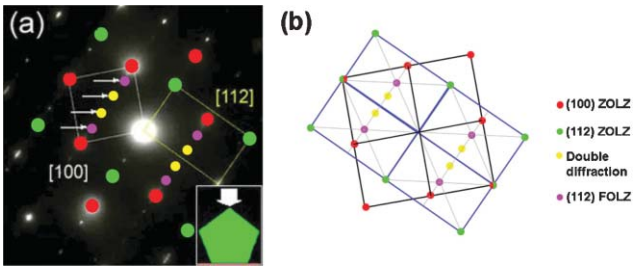

Fig. 14 (a) SAED pattern corresponding to the experimental pattern shown in Fig. 11d. Panel (b) indicates the origin of each of the spots in the aperiodic sequence of spots present in (a).

microscopy analysis of these conglomerates demonstrated that they were formed by silver nanostructures that were linked together, and many peculiar junctions among different nanowires were observed. From the SEM images shown in Fig. 15, it is clear that the branched nanostructures are composed of individual nanowires that preserve its original structure. This phenomenon might be a direct consequence of the extra energy provided by the increase in temperature; however, it is worth mentioning that branching nanowires were also observed in samples prepared at a lower temperature but to a much lesser extent. The most common type of branching is the one depicted in Fig. 15b. A more careful analysis of this kind of junction is presented in Fig. 16. By acquiring electron microscopy images in the dark field mode (panels b and c), it can be observed that the structure corresponds indeed to the junction of two independent nanowires. In this case, the nanowires were connected to each other at their tips. In other cases, we observed the presence of twist grain boundaries after two nanowires have coalesced (Fig. 17). By analyzing independently the FFT of each crystal, it can be seen that they are rotated relative to each other by 36° along the [110] direction. This observation is congruent with the fact that the nanowires have a multi-twinned pentagonal cross-section with rotational periodicity.

As expected, the particular structure of the nanowires modified their properties and behavior towards different phenomena. Recently, we studied the atmospheric corrosion of silver nanowires and nanoparticles as they are extracted from solution and exposed to laboratory air at ambient

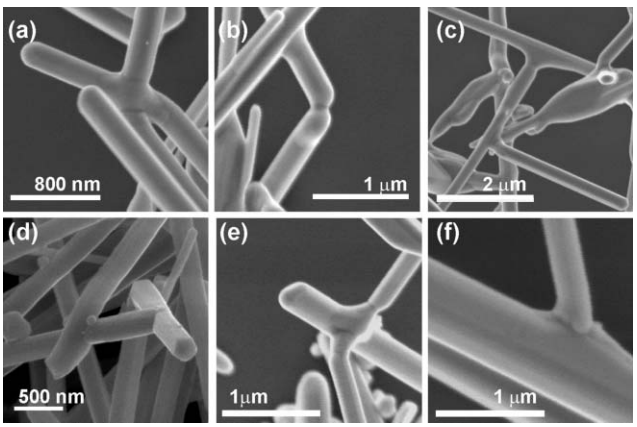

Fig. 15 Branched silver nanowires.

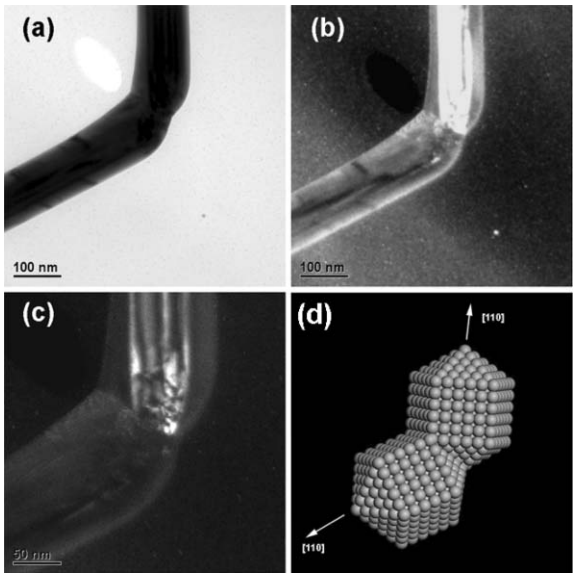

Fig. 16 Junction of two silver nanowires at their tips. (a) TEM image of the same type of junction as shown in Fig. 15b. (b, c) Dark field electron microscopy images of the junction shown in panel (a). (d) Schematic model of the junction of two nanowires through one of their {111} tip facets.

conditions.[46] Our results demonstrated that the nanowires are more susceptible to atmospheric corrosion than the single-crystalline nanoparticles and that, in both cases, a thin layer of silver sulfide nanocrystals is formed on their surfaces (Fig. 18). As regions with defects are more reactive, the corrosion process of the nanowires might be enhanced due to the existence of regions with a higher proportion of defects along

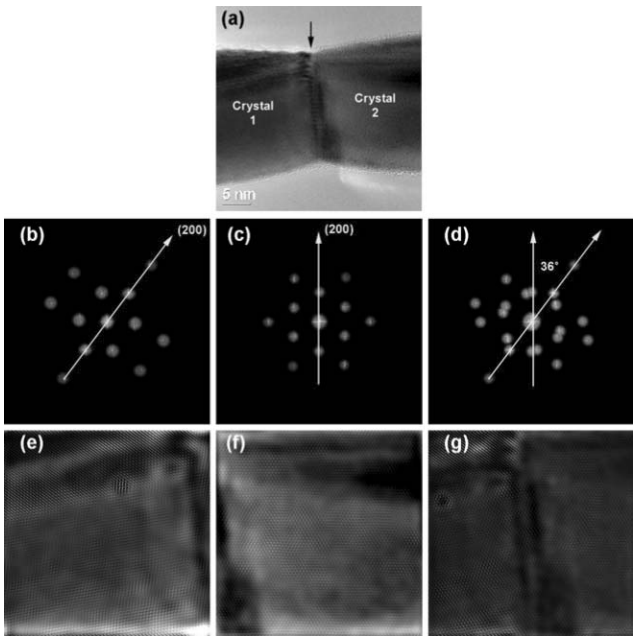

Fig. 17 Twist boundary between two silver nanowires. (a) Experimental TEM image. (b, c) Filtered FFT of crystals 1 and 2, respectively. (d) Filtered FFT of the experimental image shown in (a). (e–g) Inverse FFTs of the images shown in panels (b) to (d).

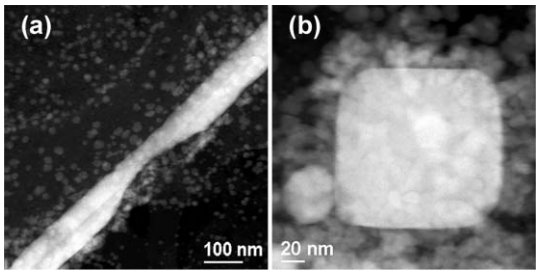

Fig. 18 High angle annular dark field (HAADF) images of (a) a silver nanowire and (b) a silver nanoparticle corroded after exposure to air at ambient conditions.

their main axis. In fact, it has been demonstrated that twinned silver particles are expected to exhibit a stronger reactivity and susceptibility towards etching than single crystalline particles.[37] Additionally, in the case of silver tarnishing, it is known that the presence of facets or steps in the silver crystal enhances the sulfidation rate;[47] thus, nucleation and growth of silver sulfide occur more rapidly along defects and dislocations than on smooth defect-free surfaces.[48] Importantly, the fact that the nanowires are highly susceptible to atmospheric corrosion might limit their use in nanofabrication and nanoelectronics.

Another important effect of the particular structure of this type of nanowire is observed in their mechanical properties. Wu *et al.* developed a general method to measure the mechanical properties of nanowires.[49] This method is based on nanowire bending under a lateral load using an atomic force microscope tip. With this approach, they analyzed the mechanical properties of the multi-twinned silver nanowires produced by the polyol method, and found that silver nanowires are stronger than bulk silver.[50] The results shown that, for nanowires with diameters from 22 to 35 nm, the average value of Young's modulus was $\sim$102 GPa, which is higher than that of bulk silver (*i.e.* 83 GPa). Surprisingly, they found that the extent of plastic deformation at failure is less than 40% of the elastic deformation. They explained that the grain orientation as well as the grain boundary organization within the nanowires is responsible for their anomalous strength and brittle fracture. As the main slip directions in the nanowire grains intersect with the twinning boundaries that run along the entire wire, a uniformly hardened structure is produced. Because of the remarkable structure of the silver nanowires (*i.e.* highly oriented nanoscale grains) produced by the polyol method, they are particularly suitable for strengthening by microstructure modification. As the growth of the wires occurs along the $<110>$ direction characterized by a slip system of four (111) slip planes along the three $<1\bar{1}0>$ directions, the five grain boundaries in this type of nanowire necessarily intersect with all of the possible slip systems and the motion of dislocations is restricted by the twinning boundaries. Hence, these nanowires are effectively grain boundary hardened materials. As shown in Fig. 19, we have qualitatively tested the mechanical properties of silver nanowires using a nanomanipulator installed in a FEI Strata DB235 double beam instrument, demonstrating that these nanowires possess interesting mechanical properties. As clearly seen in the images, the nanowires can be plastically deformed. Fig. 20

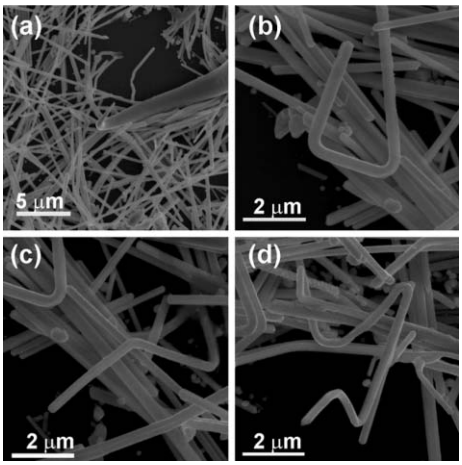

Fig. 19 Nanomanipulation of silver nanowires.

shows the same type of manipulation but on a single nanowire. In this case, one needle of the nanomanipulator was dipped in a suspension of nanowires in water. As shown in (a), at the beginning of the experiment, the original nanowire was already deformed. The origin of such a deformation might be due to the surface tension of water as it was evaporated because of the vacuum in the equipment. By carefully moving another needle of the nanomanipulator towards the nanowire, the nanowire was deformed and bent $\sim 180^{\circ}$. After that, the nanowire-free needle came into contact with the other needle and pinched off the nanowire.

As mentioned before, gold nanorods and nanowires with the same structure have been reported. In this context, the synthesis of gold nanorods by seed-mediated growth in the presence of cetyltrimethylammonium bromide (CTAB) has been pursued extensively. According to those reports, the resulting morphologies depend on the type and concentration of seed crystals used, and on the presence of surfactant molecules that promote growth in a specific crystallographic direction. In some cases, the presence of micelles acting as quasi-hard templates for the growth of the metal crystal has been widely considered as the growth mechanism. In spite of

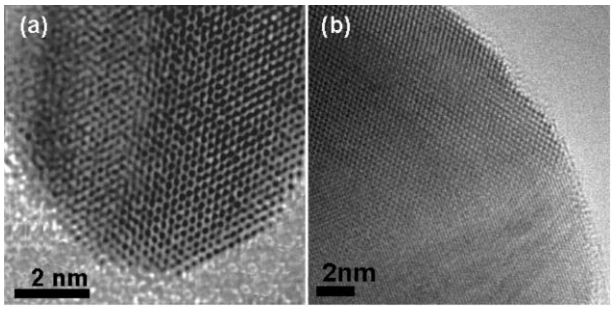

Fig. 21 (a) HRTEM image of the tip of a gold nanorod. The (111) surfaces show an expansion and a short (110) facet with (1 × 2) reconstruction is observed. (b) Cs-corrected HRTEM image of the tip of a silver nanowire. The presence of monoatomic surface steps is clearly visible.

that, it is difficult to imagine that rod-like micelles exist through the entire length scale for the metal crystal to growth. In fact, micelles in solution are not static and are constantly formed and broken; thus, kinetics and twinning play important roles in the formation of the original nuclei that promote crystal anisotropy.

In a recent work Liu and Guyot-Sionnest[51] have grown nanorods and nanowires promoted with Ag(I). The silver seeds promote the growth of {110} facets for the gold nanorods. These authors clearly show that the seed mediated growth of gold nanostructures strongly depends on the structure of the seed.

Previously, we have produced gold nanorods by reducing potassium tetrachloroaurate ($KAuCl_4$) by using fresh alfalfa (Medicago Sativa).[11] In this method, after the biomass is milled and saturated with the gold precursor, gold nanoparticles and nanorods are produced. In this case, no additional capping agents such as CTAB were used. TEM analysis demonstrated that these nanorods possess the same five-fold multi-twinned structure. HRTEM images demonstrated the presence of surface relaxation, faceting steps and surface reconstruction (Fig. 21a).[43] In particular, a distortion of $\sim 20\%$ with respect to the bulk gold lattice parameter in the (111) surface was measured, while in the case of the (100)

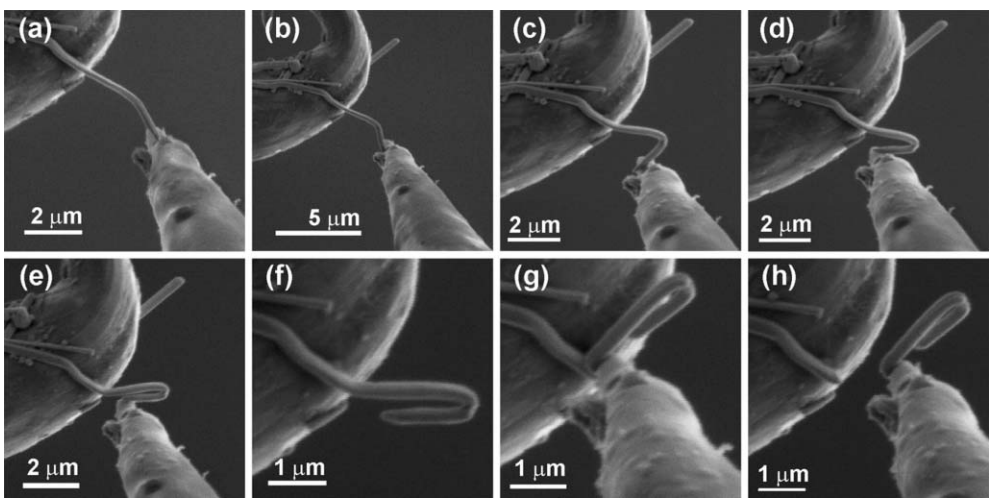

Fig. 20 Nanomanipulation of a single silver nanowire.

surface a variable surface expansion between 10% and 15% with respect to the bulk gold lattice parameter was also observed. Additionally, at the tips, it was also possible to observe a (1 × 2) reconstructed (110) facet. Monoatomic surface steps along the [110] direction were also detected. In the case of the silver nanowires produced by the polyol method, the use of Cs-corrected TEM allowed us to eliminate the delocalization of the image and true images of the surfaces were obtained. Again, the presence of monoatomic steps and surface relaxation is clear (Fig. 21b).

3.2.3 Branched nanoparticles. Recently, the first branched gold nanostructures were reported.[52] The initial production methods employed for this type of structure were derived from the seed-mediated growth technique for the synthesis of gold nanorods. According to those reports, the morphology of the resulting crystals depended on the size, shape, and type (*i.e.* gold or silver) of seed crystals used, the relative concentrations of the components, as well as on the number and duration of incubation steps employed. On the other hand, we have found that branched gold nanocrystals can also be obtained by colloidal reduction with ascorbic acid without the use of seed crystals, surfactant molecules, or successive incubation steps.[53] Once more, this is an indication that the fundamental processes that govern the production of anisotropic crystals are not only related to the use of guiding capping agent molecules.

In this case, we identified two main distinct types of star polyhedral nanocrystals, corresponding to icosahedra and cuboctahedra with preferential growth of their exposed {111} surfaces (Fig. 22). Specifically, the {111} faces of the original Archimedean solids grew into tetrahedral pyramids, with the base of each pyramid being the original polyhedral face. In the case of the cuboctahedrally-derived star nanocrystals, the nuclei were monocrystalline cuboctahedral nanoparticles with eight pyramids growing out from their {111} exposed surfaces, while in the case of the icosahedrally-derived star nanocrystals, the nuclei were five-fold twinned nanocrystals with twenty pyramids growing out from each of the {111} surfaces; hence, the crystal shape closely resembles a great stellated dodecahedron, one of the Kepler–Poinsot solids. In most cases, the pyramids were single crystals and almost no defects were observed. However, a common defect for multiple-twinned stars was the presence of a localized twin boundary within a pyramid, while in the monocrystalline stars stacking faults extending through the entire crystal were sometimes observed (Fig. 23).

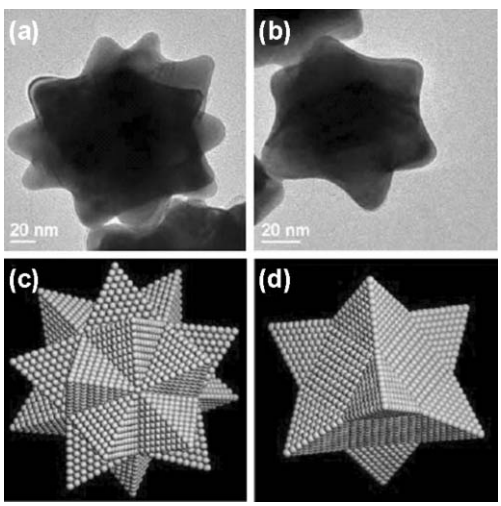

Fig. 22 TEM images of (a) an icosahedrally-derived and (b) a cuboctahedrally-derived branched gold nanoparticle. (c, d) Schematic models of such nanocrystals.

By foregoing the use of surfactant molecules and seed crystals during the synthesis, the size and shape distribution of the products was not as nicely controlled as in the case where these extra components are used. Therefore, it is reasonable to suggest that surfactants truly assist in the production of specific anisotropic shapes. However, as mentioned before, the fundamental mechanism for anisotropic growth also involves nucleation and kinetics of the reaction, as demonstrated by the presence of branched nanoparticles in the absence of surfactants.

Finally, with a different approach, we synthesized platinum powders by the polyol method using PDDA as capping agent.[39] For the minimum amount of PDDA tested, once the reaction was stopped, a fine black precipitate was observed. TEM showed that the powder was mainly composed by amorphous aggregates of small nanocrystals of about 7 nm in average diameter. Interestingly, we also observed the presence of branched nanocrystals with very special morphologies including arrow- and star-shaped nanoparticles among others. Importantly, branched nanoparticles were only formed when a high reduction rate and supersaturating conditions were accomplished, suggesting that the role of the capping agent in promoting these structures was minimal. Analysis of TEM images demonstrated that the components of the branched crystals are crystallites in twin relationship resulting in the peculiar shapes observed. Again, in some cases, the nuclei crystals were multi-twinned nanoparticles; however, also core crystals with an fcc-type of structure such as the truncated octahedron were also observed. High-resolution TEM (Fig. 24b) of some of these nanoparticles showed that typically their arms are single crystals growing in the [110] direction with lattice spacing between the {111} planes of 0.23 nm, which is consistent with bulk Pt. By combining the information provided by high angle annular dark field (HAADF) images with the information obtained from HRTEM images of the same nanoparticle, a schematic model of the particle can be

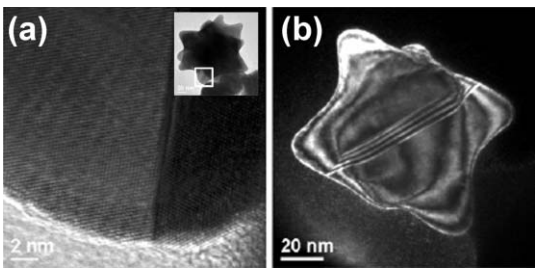

Fig. 23 (a) HRTEM image of the twin observed in one of the pyramids of the icosahedrally-derived gold nanoparticle shown in the inset. (b) Weak-beam dark field electron microscopy image of a cuboctahedrally-derived gold nanocrystal with stacking faults extending through the entire particle.

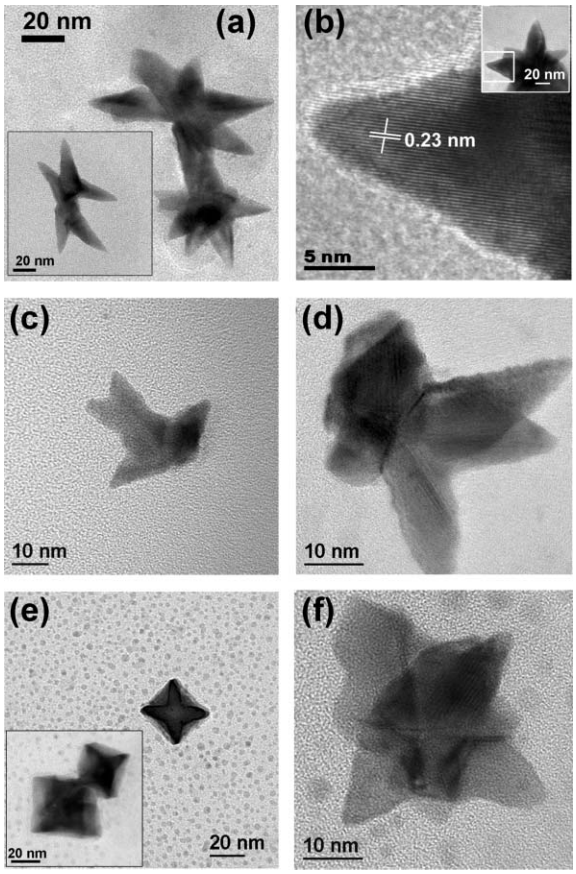

Fig. 24 TEM images of different types of platinum branched nanoparticles. The image shown in (b) corresponds to a high-resolution TEM image of the region enclosed in the corresponding inset. The interplanar spacing of 0.23 nm corresponds to the {111} planes for bulk Pt.

produced. The model has a truncated octahedron as seed with eight pyramids growing from each truncation in the [110] direction. Briefly, the contrast observed in HAADF images is mainly proportional to Z^2, while the intensity of the image is related to the number of electrons scattered and the probability that an electron interacts with the nucleus of an atom is directly proportional to the thickness of the sample. Since the atomic weight of platinum is significantly larger than the atoms that compose the PDDA coating (*i.e.* C, N and H), the atomic weight throughout the particle can be considered constant; so the differences in intensities observed in HAADF images of the nanoparticles will be mostly due to the differences in thickness of the particle. Therefore, by plotting in 3D an intensity profile, topographical information can be obtained. An example of this is shown in Fig. 25b, where the intensity profile observed in a HAADF image of a platinum nanoparticle with the morphology shown in Fig. 24e was produced, showing that the nanoparticle indeed has protuberances at each corner.

4. Conclusions

According to the literature, in the case of noble metals, it appears that there is not a general mechanism responsible for

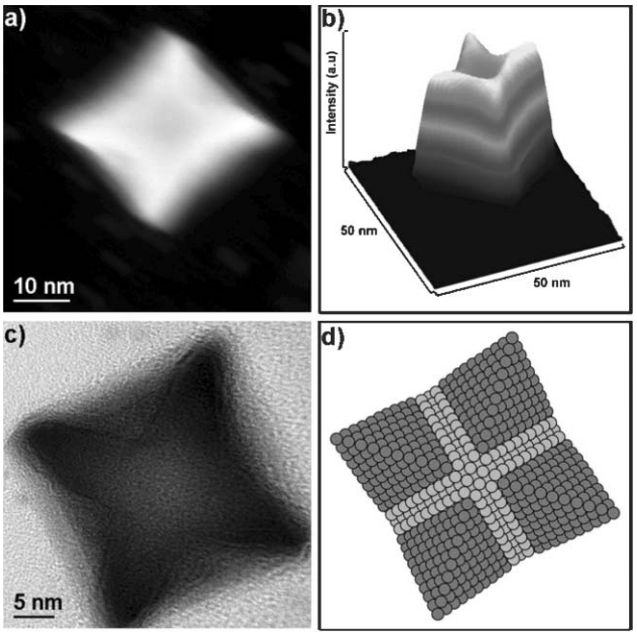

Fig. 25 (a) HAADF image of the same type of branched nanoparticles shown in Fig. 24e. (b) 3D Intensity profile of the HAADF image shown in (a). (c) Bright field TEM image of the same type of nanoparticle. (d) Schematic model of the particle.

the formation of anisotropic nanostructures and specific issues for each particular reaction environment need to be considered. The role of each reaction parameter in the formation of such crystals is not yet fully understood and it has been proposed that the final shape of the nanocrystals depends on different factors operating synergistically. A common point in many different reports highlights the important role of surfactants and capping agent molecules as directing agents for achieving anisotropic growth. However, as discussed in this feature article, important considerations regarding the nucleation kinetics as well as the formation of twin planes that favor anisotropic structures should be also taken into account. Twins are readily formed during nucleation of colloidal noble-metal nanocrystals; hence, strategies to control the kinetics and formation of particular nuclei should provide better ways for rational strategies to produce anisotropic noble metal nanocrystals.

It should be pointed out that in some cases the surfactant stabilization seems to have a more important role. This is a question open for future work. Other open questions are for instance why twinning seems to be playing a lesser role in other metals such as Pt and an intermediate role in metals such as Pd. Differences in twinning energy are not sufficient to explain this problem.

Acknowledgements

The authors are indebted to the Welch Foundation for financial support through the grant F-1615, and to DARPA (HR0011-06-1-0005). We also acknowledged support from the NSF through the grant "Alloys at the Nanoscale: The Case of Nanoparticles". We are also indebted to the ICNAM at UT Austin for support.

The authors acknowledge Rodrigo Velazquez for acquiring some of the dark field TEM images, as well as Domingo Garcia Gutierrez for helping with the nanomanipulation experiments. JLE acknowledges the support received by CONACYT-Mexico.

References

1 M.-C. Daniel and D. Astruc, *Chem. Rev.*, 2004, **104**, 293–346.
2 N. L. Rosi and C. A. Mirkin, *Chem. Rev.*, 2005, **105**, 1547–1562; J. L. Elechiguerra, J. L. Burt, J. R. Morones, A. Camacho-Bragado, X. Gao, H. H. Lara and M. J. Yacaman, *J. Nanobiotechnol.*, 2005, **3**, 6; J. R. Morones, J. L. Elechiguerra, A. Camacho, K. Holt, J. B. Kouri, J. T. Ramirez and M. J. Yacaman, *Nanotechnology*, 2005, **16**, 2346–2353.
3 C. Burda, X. Chen, R. Narayanan and M. A. El-Sayed, *Chem. Rev.*, 2005, **105**, 1025–1102.
4 L. M. Liz-Marzan, *Mater. Today*, 2004, **7**, 26–31; I. O. Sosa, C. Noguez and R. G. Barrera, *J. Phys. Chem. B*, 2003, **107**, 6269–6275.
5 J. J. Mock, M. Barbic, D. R. Smith, D. A. Schultz and S. Schultz, *J. Chem. Phys.*, 2002, **116**, 6755–6759.
6 C. Murphy, T. Sau, A. Gole and C. Orendorff, *Mater. Res. Bull.*, 2005, **30**, 349–355.
7 R. Narayanan and M. A. El-Sayed, *Nano Lett.*, 2004, **4**, 1343–1348; R. Narayanan and M. A. El-Sayed, *J. Am. Chem. Soc.*, 2004, **126**, 7194–7195.
8 Y. Xia and N. Halas, *Mater. Res. Bull.*, 2005, **30**, 338–348.
9 E. Leontidis, K. Kleitou, T. Kyprianidou, V. Bekiari and P. Lianos, *Langmuir*, 2002, **18**, 3659.
10 Y.-Y. Yu, S.-S. Chang, C.-L. Lee and C. R. C. Wang, *J. Phys. Chem. B*, 1997, **101**, 6661–6664.
11 G. Canizal, J. A. Ascencio, J. Gardea-Torresday and M. Jose-Yacaman, *J. Nanopart. Res.*, 2001, **3**, 475–481.
12 N. R. Jana, L. Gearheart and C. J. Murphy, *J. Phys. Chem. B*, 2001, **105**, 4065–4067.
13 N. R. Jana, L. Gearheart and C. J. Murphy, *Chem. Commun.*, 2001, 617–618.
14 Y. Sun and Y. Xia, *Adv. Mater.*, 2002, **14**, 833–837.
15 J.-Q. Hu, Q. Chen, Z.-X. Xie, G.-B. Han, R.-H. Wang, B. Ren, Y. Zhang, Z.-L. Yang and Z.-Q. Tian, *Adv. Funct. Mater.*, 2004, **14**, 183–189.
16 F.-K. Liu, P.-W. Huang, Y.-C. Chang, C.-J. Ko, F.-H. Ko and T.-C. Chu, *J. Cryst. Growth*, 2005, **273**, 439–445.
17 I. Lisiecki, A. Filankembo, H. Sack-Kongehl, K. Weiss, M. P. Pileni and J. Urban, *Phys. Rev. B*, 2000, **61**, 4968–4974.
18 I. Lisiecki, H. Sack-Kongehl, K. Weiss, J. Urban and M. P. Pileni, *Langmuir*, 2000, **16**, 8802–8806.
19 R. Jin, Y. Cao, C. Mirkin, K. Kelly, G. Schatz and J. Zheng, *Science*, 2001, **294**, 1901; M. Maillard, S. Giorgio and M. Pileni, *Adv. Mater.*, 2002, **14**, 1084; I. Pastoriza-Santos and L. Liz-Marzan, *Nano Lett.*, 2002, **2**, 903; Y. Sun, B. Mayers and Y. Xia, *Nano Lett.*, 2003, **3**, 675.
20 G. Bogels, H. Meekes and P. Bennema, *J. Phys. Chem. B*, 1999, **103**, 7577–7583.
21 C. Lofton and W. Sigmund, *Adv. Funct. Mater.*, 2005, **15**, 1197–1208.
22 M. J. Yacaman, J. A. Ascencio, H. B. Liu and J. Gardea-Torresdey, *J. Vac. Sci. Technol., B*, 2001, **19**, 1091–1103.
23 N. Doraiswamy and L. D. Marks, *Surf. Sci.*, 1996, **348**, 67–69; S. Iijima and T. Ichihashi, *Phys. Rev. Lett.*, 1986, **56**, 616–619; D. J. Smith, A. K. Petford-Long, L. R. Wallenberg and J.-O. Bovin, *Science*, 1986, **233**, 872–875; H. B. Liu, J. A. Ascencio, M. Perez-Alvarez and M. J. Yacaman, *Surf. Sci.*, 2001, **491**, 88–98.
24 B. Wiley, Y. Sun, B. Mayers and Y. Xia, *Chem.–Eur. J.*, 2005, **11**, 454–463.
25 M.-P. Pileni, *Nat. Mater.*, 2003, **2**, 145–150.
26 S. Ino, *J. Phys. Soc. Jpn.*, 1969, **27**, 941–953.
27 K. Heinemann, M. J. Yacaman, C. Y. Yang and H. Poppa, *J. Cryst. Growth*, 1979, **47**, 177–186; A. Howie and L. D. Marks, *Philos. Mag. A*, 1984, **49**, 95–109.
28 B. Pauwels, D. Bernaerts, S. Amelinckx, G. Van Tendeloo, J. Joutsensaari and E. I. Kauppinen, *J. Cryst. Growth*, 1999, **200**, 126–136.
29 U. Dahmen and K. H. Westmacott, *Science*, 1986, **233**, 875–876; H. Hofmeister and T. Junghanns, *Mater. Sci. Forum*, 1993, **113–115**, 631–636.
30 S. Ino and S. Ogawa, *J. Phys. Soc. Jpn.*, 1967, **22**, 1365–1374.
31 L. D. Marks and D. J. Smith, *J. Cryst. Growth*, 1981, **54**, 425–432; L. D. Marks, *Philos. Mag. A*, 1984, **49**, 81–93; L. D. Marks, *Rep. Prog. Phys.*, 1994, **57**, 603–649.
32 C. Cleveland and U. Landman, *J. Chem. Phys.*, 1991, **94**, 7376–7396.
33 F. Kim, S. Connor, H. Song, T. Kuykendall and P. Yang, *Angew. Chem.*, 2004, **116**, 3759.
34 U. Dahmen, C. Hetherington, V. Radmilovic, E. Johnson, S. Xiao and C. Luo, *Microsc. Microanal.*, 2002, **8**, 247–256.
35 H. Hofmeister, Fivefold Twinned Nanoparticles, in *Handbook of Nanotechnology*, ed. H. Naiwa, American Scientific Publishers, California, USA, 2004.
36 D. V. Goia and E. Matijevic, *New J. Chem.*, 1998, **22**, 1203–1215.
37 S. I. Hyuk, Y. T. Lee, B. Wiley and Y. Xia, *Angew. Chem., Int. Ed.*, 2005, **44**, 2154–2157.
38 J. Chen, T. Herricks, M. Geissler and Y. Xia, *J. Am. Chem. Soc.*, 2004, **126**, 10854–10855; F. Bonet, V. Delmas, S. Grugeon, R. Herrera Urbina, P.-Y. Silvert and K. Tekaia-Elhsissen, *Nanostruct. Mater.*, 1999, **11**, 1277–1284; F. Bonet, S. Grugeon, L. Dupont, R. Herrera Urbina, C. Guery and J. M. Tarascon, *J. Solid State Chem.*, 2003, **172**, 111–115; K. Tekaia-Elhsissen, F. Bonet, P.-Y. Silvert and R. Herrera-Urbina, *J. Alloys Compd.*, 1999, **292**, 96–99; D. I. Garcia-Gutierrez, C. E. Gutierrez-Wing, L. Giovanetti, J. M. Ramallo-Lopez, F. G. Requejo and M. Jose-Yacaman, *J. Phys. Chem. B*, 2005, **109**, 3813–3821.
39 J. Elechiguerra, L. Larios-Lopez and M. Jose-Yacaman, *Appl. Phys. A*, 2006, **84**, 11–19.
40 R. de Wit, *J. Phys. C: Solid State Phys.*, 1972, **5**, 529–534.
41 N. W. Johnson, *Can. J. Math.*, 1966, **18**, 169–200.
42 A. J. Melmed and D. O. Hayward, *J. Chem. Phys.*, 1959, **31**, 545–546.
43 M. Jose Yacaman, J. A. Ascencio and G. Canizal, *Surf. Sci.*, 2001, **486**, L449–L453.
44 C. J. Johnson, E. Dujardin, S. A. Davis, C. J. Murphy and S. Mann, *J. Mater. Chem.*, 2002, **12**, 1765–1770; Y. Sun, B. Mayers, T. Herricks and Y. Xia, *Nano Lett.*, 2003, **3**, 955–960; H. Chen, Y. Gao, H. Zhang, L. Liu, H. Yu, H. Tian, S. Xie and J. Li, *J. Phys. Chem. B*, 2004, **108**, 12038–12043; C. Ni, P. A. Hassan and E. W. Kaler, *Langmuir*, 2005, **21**, 3334–3337; H. Hofmeister, S. A. Nepijko, D. N. Ievlev, W. Schulze and G. Ertl, *J. Cryst. Growth*, 2002, **234**, 773–781.
45 J. Reyes-Gasga, J. L. Elechiguerra, C. Liu, A. Camacho-Bragado, J. M. Montejano-Carrizales and M. J. Yacaman, *J. Cryst. Growth*, 2006, **286**, 162–172.
46 J. L. Elechiguerra, L. Larios-Lopez, C. Liu, D. Garcia-Gutierrez, A. Camacho-Bragado and M. J. Yacaman, *Chem. Mater.*, 2005, **17**, 6042–6052.
47 J. G. Allpress and J. V. Sanders, *Philos. Mag.*, 1964, **10**, 827–836; H. Schloetterer, *Phys. Status Solidi*, 1965, **11**, 219–229.
48 A. J. Forty and F. C. Frank, *Proc. R. Soc. London, Ser. A*, 1953, **217**, 262–270.
49 B. Wu, A. Heidelberg and J. J. Boland, *Nat. Mater.*, 2005, **4**, 525–529.
50 B. Wu, A. Heidelberg, J. J. Boland, J. Sader, X. Sun and Y. Li, *Nano Lett.*, 2006, **6**, 468–472.
51 M. Liu and P. Guyot-Sionnest, *J. Phys. Chem. B*, 2005, 22192–22200.
52 S. Chen, Z. L. Wang, J. Ballato, S. H. Foulger and D. L. Carroll, *J. Am. Chem. Soc.*, 2003, **125**, 16186–16187; T. K. Sau and C. J. Murphy, *J. Am. Chem. Soc.*, 2004, **126**, 8648–8649.
53 J. L. Burt, J. L. Elechiguerra, J. Reyes-Gasga, J. Martin Montejano-Carrizales and M. Jose-Yacaman, *J. Cryst. Growth*, 2005, **285**, 681–691.